5. RADIONUCLIDE MOBILITIES

Americium

Breakthrough curves for americium under the influence of the PWS (*i.e.* with HA and EDTA) (solid circles) are given in Figure 5.1. The dashed line is the ratio of C/C_0 approximately corresponding to background (extrinsic and intrinsic). The breakthrough curves were substantially different from those presented in the previous section for strontium. Whereas the strontium breakthrough curves were characterized by a single peak containing essentially all of the activity in the spike, the americium curve was characterized by three fractions having distinctly different mobilities. There was a very small, high mobility component (<<1%) that emerged from the column within the first few pore volumes, an intermediate mobility component (≈50%) that emerged between 3 and 500 pore volumes, and a low mobility component (≈50%) that did not emerge and was retained in the first 3 cm of the column. It is convenient to operationally define the fraction emerging in less than 3 DPV as high mobility, 3-500 DPV as intermediate mobility, and greater than 500 DPV as low mobility. Since similar behavior was observed for thorium, plutonium(IV), and neptunium, these definitions are also applied to their behavior, although the appropriate upper limit for the low mobility component varies somewhat.

Also shown in Figure 5.1 are breakthrough curves for americium under the influence of the modified perched water simulant (MPWS), *i.e.* with HA and EDTA removed. Two tests were conducted, one with a fresh spike and one with a spike aged for 24 hours. The breakthrough curves for the two spikes were essentially the same, and they were very similar to the PWS curve for the first few pore volumes. However, they differed dramatically from the PWS curve between 3 and 500 DPV, where the intermediate mobility component almost disappeared. The fractions and retardation factors for the intermediate mobility component are compared in Table 5.1.

The high mobility portion of the breakthrough curves is expanded in Figure 5.2, where data from a total of six experiments are presented. The additional data include two replicates of the fresh spike and an experiment in which the spike concentration was increased by approximately a factor of ten (denoted "high C_0"). The breakthrough curves in the high mobility region and the recoveries for the high mobility component (Table 5.2) were surprisingly reproducible even though the concentrations in the effluent were a

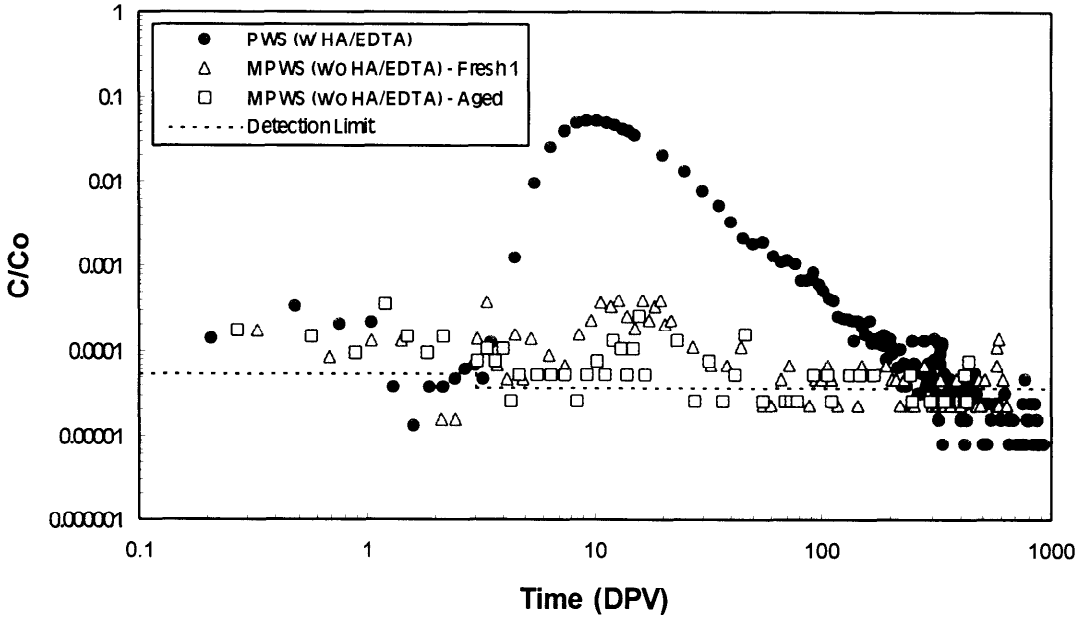

Figure 5.1. Americium breakthrough curves

Table 5.1. Recoveries and Retardation Factors for the Americium Intermediate Mobility Component

Simulant	Recovery (3–500 DPV)	Retardation Factor
PWS	0.5000	16
MPWS– Fresh Spike	0.0012	18
MPWS– Aged Spike	0.0003	18

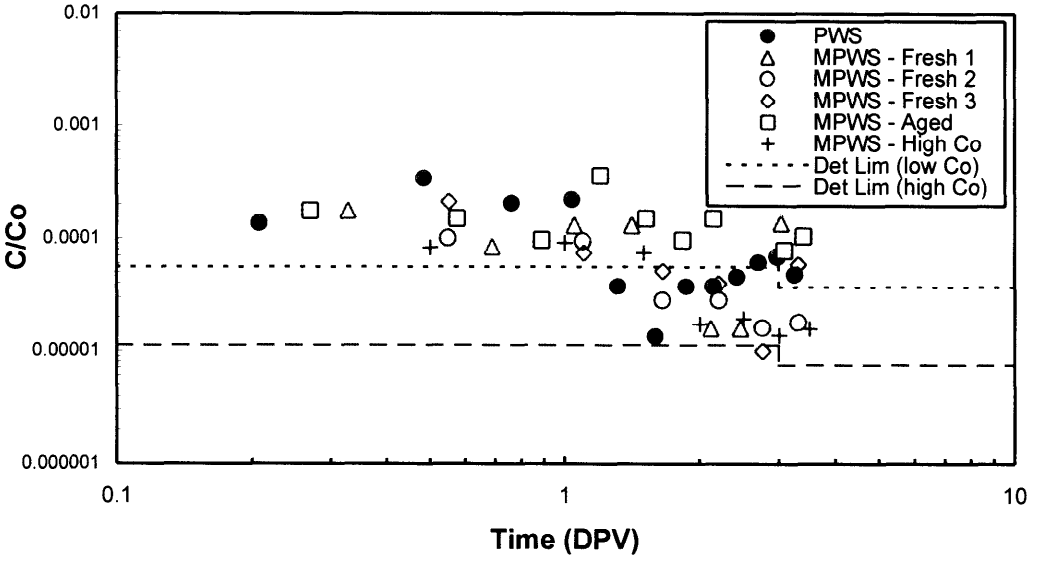

Figure 5.2. Expanded view of high mobility time period for americium

Table 5.2. Recoveries for the Americium High Mobility Component

Simulant	Recovery (<3 DPV)
PWS	0.00023
MPWS – Fresh Spike (1)	0.00031
MPWS – Aged Spike	0.00041
MPWS – Fresh Spike (2)	0.00013
MPWS – Fresh Spike (3)	0.00020
MPWS High C_0	0.00013

factor of 10,000 lower than those in the spike and there was considerable scatter in the data. Two detection limits are included in the graph, one for experiments conducted with the typical spike concentration (labeled "low C_0") and one for the experiment conducted with an elevated spike concentration (labeled "high C_0"). Below 1 DPV, the concentrations in the "high C_0" experiment were almost an order of magnitude above the detection limit. The "high C_0" data resulted from an experiment to improve the precision of the high mobility portion of the breakthrough curve by increasing the americium concentration in the spike by an order of magnitude. The results are shown in Figure 5.3, where uncertainty estimates due to counting error (one standard deviation) are included. These data confirmed that the high mobility component was statistically different from background. Here, the C/C_0 corresponding to background was approximately 1×10^{-6}, and the effluent concentrations in the first 3 DPV were between one and two orders of magnitude higher. Also included in Figure 5.3 are analyses of selected effluent fractions filtered to 3 nm. The filtered and unfiltered concentrations were essentially the same, indicating that the high mobility component was either in a soluble or very small particulate (<3 nm) form.

From a predominance area diagram for the americium (III) hydroxide-carbonate system (E_H vs pH) (Appendix A), americium is predicted to exist as solid $Am_2(CO_3)_3$ species. Batch filtration experiments (Figure 5.4 and Appendix F) were qualitatively consistent with these predictions as the americium was quickly converted to a particulate form. Immediately following preparation of the spike, over 80% of the americium was in a particulate form larger than 3 nm, and after 24 hours, the fraction increased to almost 100%.

These data suggest the following conceptual model for americium. Americium transport in the columns is driven by its extremely low solubility and the formation of americium carbonate precipitates which are likely filtered mechanically[1]. The high mobility component could be either soluble $Am_2(CO_3)_3$ or a particulate form which penetrates the soil matrix.

Thorium and Plutonium(IV)

The breakthrough curves for thorium under the influence of the PWS (solid circles in

[1] In a series of experiments described in Appendix D, it was observed that colloids, both "true" and "associated", are attenuated by the soil matrix.

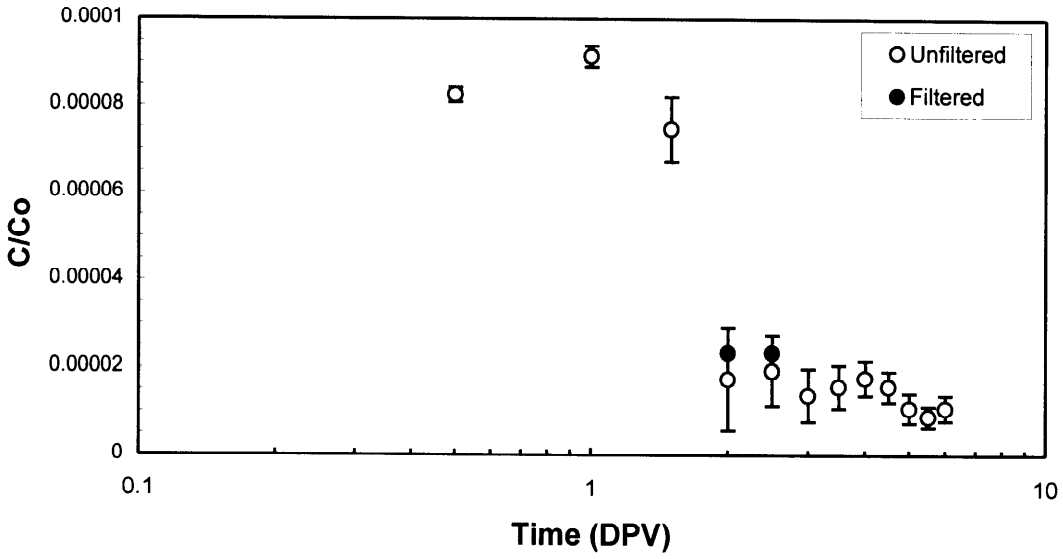

Figure 5.3. Americium high mobility component for an elevated C_0 – unfiltered and filtered (> 3 nm) analyses

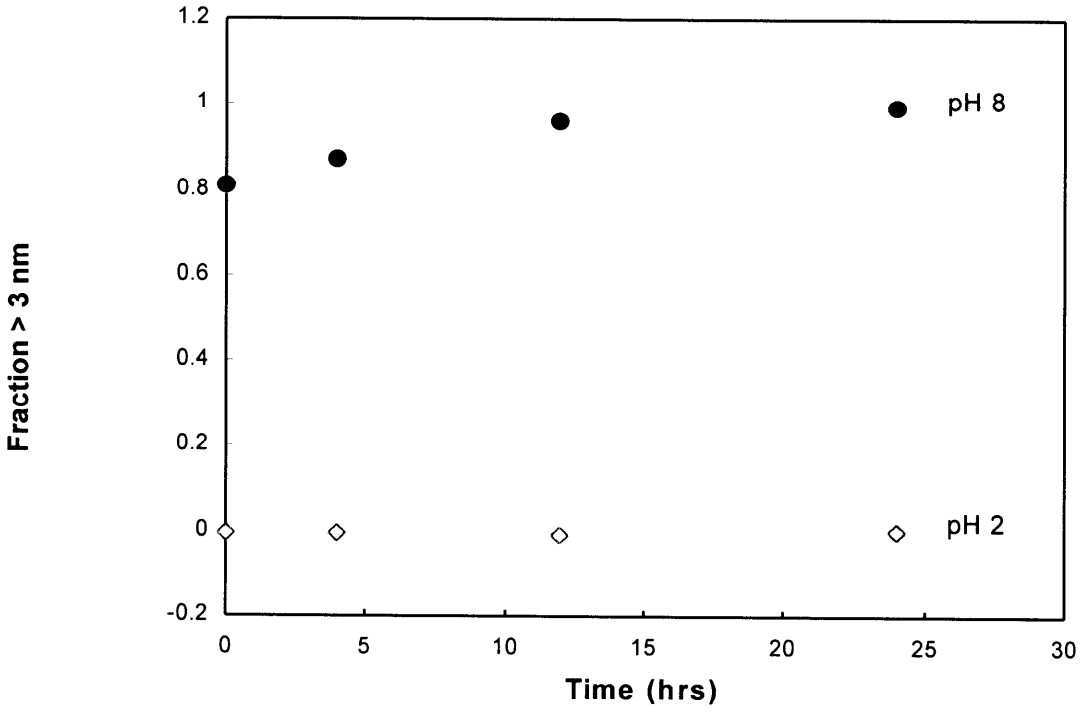

Figure 5.4. Particulate fraction as a function of aging time for americium

Figure 5.5) and MPWS (open symbols in Figure 5.5) were similar to americium. For the PWS, there was a very small, high mobility component (<<1%) that emerged from the column within the first few pore volumes and a large intermediate mobility component that emerged between 3 and 500 pore volumes. The remainder of the thorium was retained in the column. For the MPWS, the intermediate mobility component almost disappeared, with the fractional recovery decreasing from almost 0.3 to less than 0.001 (Table 5.3). The high mobility component also declined, with the concentrations falling below the estimate of the detection limit. However, as noted previously, the detection limit is likely an over estimate. When the 0.1 to 10 DPV time period is expanded, and results of additional experiments focused on this region are added to the two experiments shown in Figure 5.5, the breakthrough curves are surprisingly reproducible (Figure 5.6). This reproducibility is also evident in the fractional recoveries (Table 5.4), which vary over less than an order of magnitude for the MPWS (with the normal silica concentration). If thorium from the spike was absent from the effluent, the fractional recoveries would vary about zero. More conclusive evidence regarding the existence of a high mobility component for thorium is found in the "high C_0" experiment, where there was a well-defined peak extending from 1 to 6 DPV (Figures 5.6 and 5.7), and the recovery showed reasonable agreement with those for the other MPWS experiments (Table 5.4). These results suggest a high mobility component for thorium on the order of 10^{-5}, and the filtration analyses indicate that all of it was in a particulate form larger than 3 nm. This is consistent with the batch filtration results (Figure 5.8), which showed thorium to be entirely in a particulate form almost immediately after preparation of the spike. Since the PWS and MPWS were both oversaturated with respect to silica, it is possible that the particulate thorium was actually a thorium species sorbed to SiO_2 precipitates. Also included in Table 5.4 are results for experiments conducted with silica concentrations below saturation (denoted as "low Si"). The fractional recoveries for these tests were higher than for the tests with silica above saturation, suggesting that production of the thorium high mobility component may involve competition among more than one process.

The breakthrough curves for plutonium(IV) (Figure 5.9) under the influence of the PWS (solid symbols) and MPWS (open symbols) were similar to thorium and americium. There was a very small, high mobility component (<<1%) that emerged from the column within the first few pore volumes and a large intermediate mobility component (≈50%)

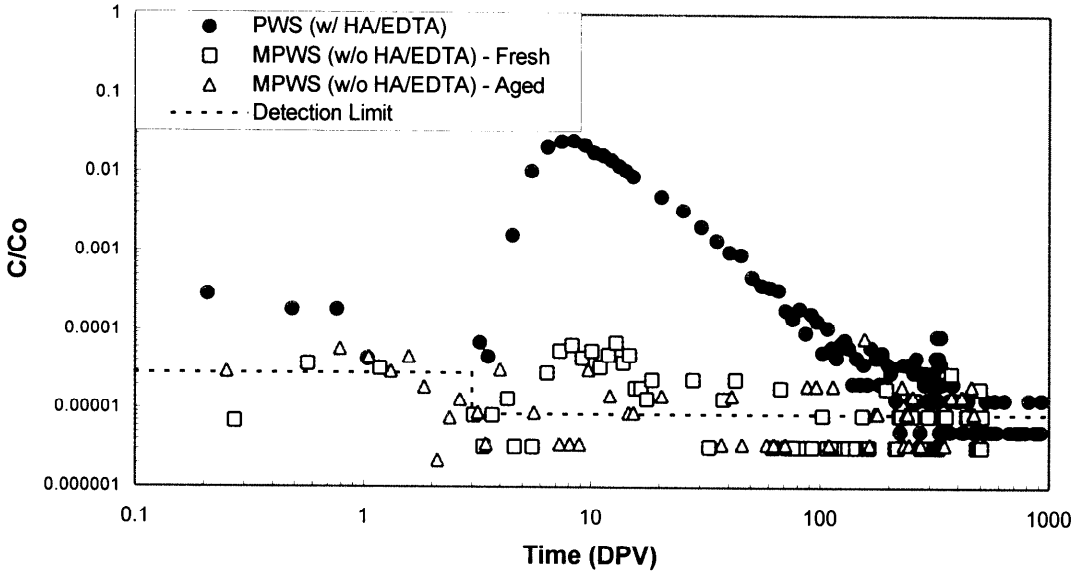

Figure 5.5. Thorium breakthrough curves

Table 5.3. Recoveries and Retardation Factors for the Thorium Intermediate Mobility Component

Simulant	Recovery (2.5 – 500 DPV)	Retardation Factor
PWS	0.27000	23
MPWS – Fresh Spike	0.00088	NA*
MPWS – Aged Spike	0.00070	NA*

*NA – not applicable

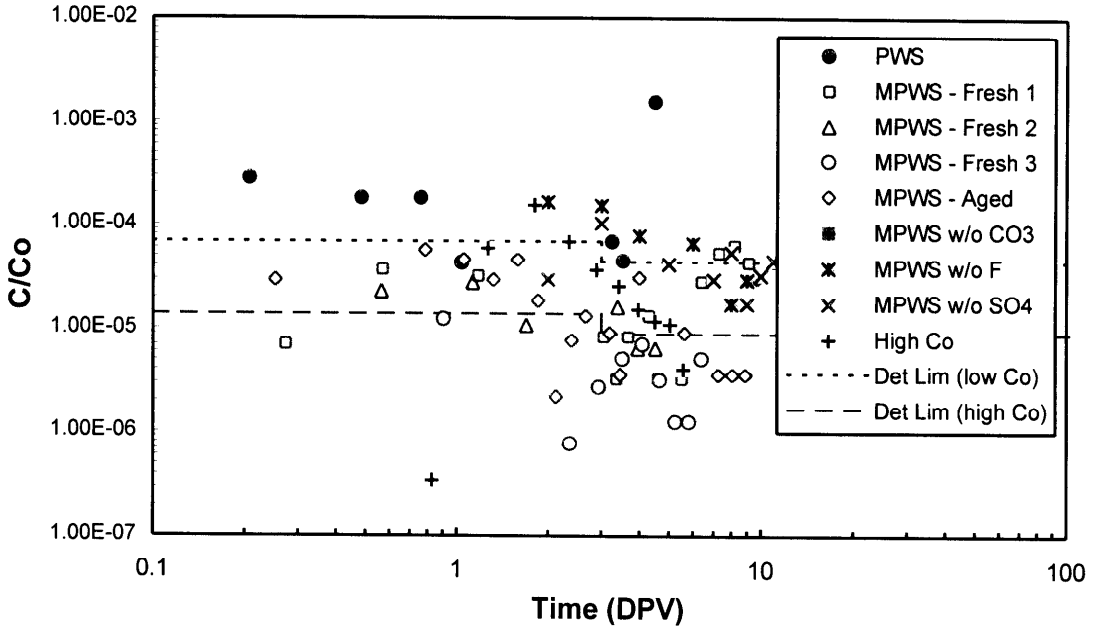

Figure 5.6 Expanded view of high mobility time period for thorium

Table 5.4. Recoveries for the Thorium High Mobility Component

Simulant	Recovery (<6 DPV)
PWS	0.000140
MPWS – Fresh Spike 1	0.000009
MPWS – Fresh Spike 2	0.000032
MPWS – Fresh Spike 3	0.000013
MPWS – Aged Spike	0.000063
MPWS – High C_0	0.000014
MPWS w/o CO_3^{2-} (low Si)	0.000100
MPWS w/o F^- (low Si)	0.000250
MPWS w/o SO_4^{2-} (low Si)	0.000180

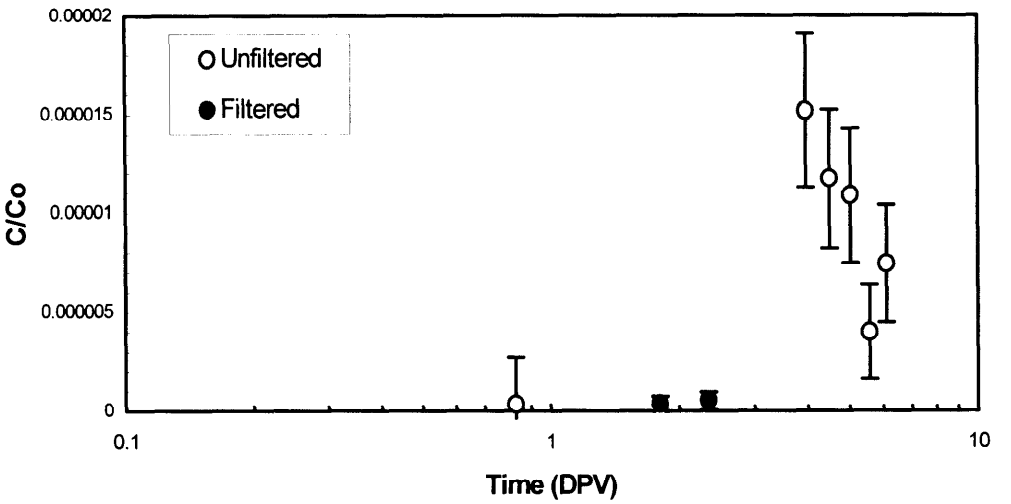

Figure 5.7. Thorium high mobility component for an elevated C_0 – unfiltered and filtered (> 3 nm) analyses

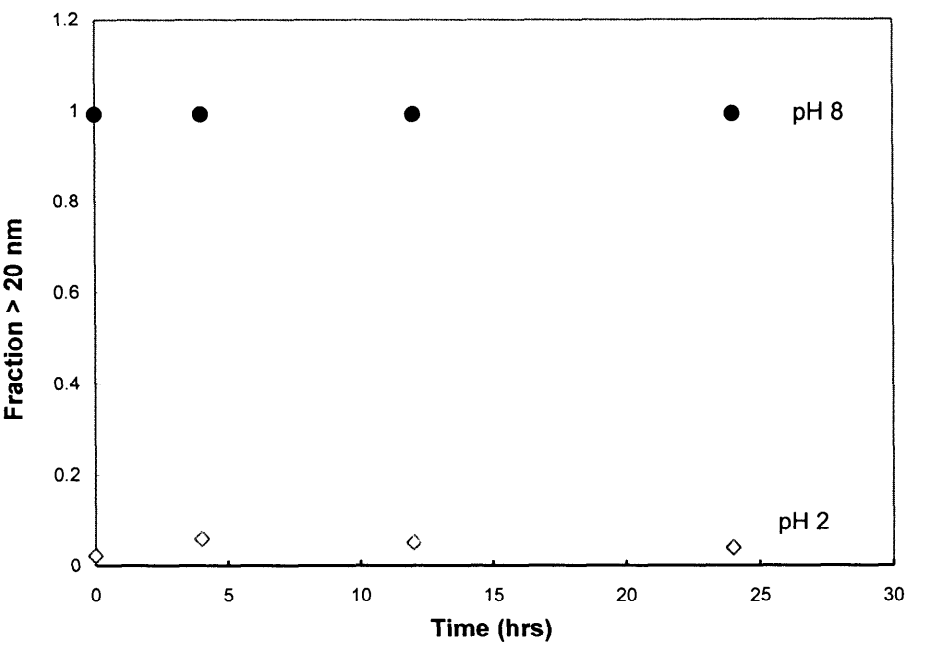

Figure 5.8. Particulate fraction as a function of aging time for thorium

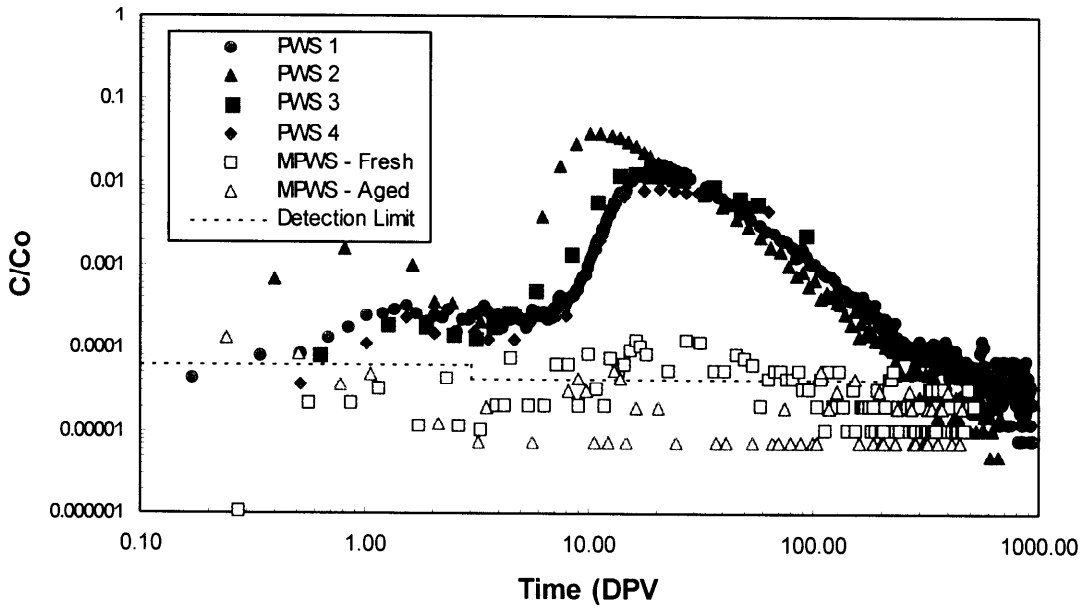

Figure 5.9. Plutonium(IV) breakthrough curves

that emerged between 3 and 500 pore volumes. The remainder of the plutonium(IV) did not emerge from the column within the first 1000 DPV. For the MPWS, distinct high and intermediate mobility components were not observed, although there appeared to be uniform, non-zero breakthrough throughout the experiment. Recoveries and retardation factors for the 3–1000 DPV time period are given in Table 5.5.

The 0.1 to 10 DPV time period is expanded in Figure 5.10 for the PWS and in Figure 5.11 for the MPWS. For the PWS experiments, the measurements during this time period were above the detection limit and were about an order of magnitude above background. The recoveries varied considerably, ranging from 10^{-3} to 10^{-5} (Table 5.6). For the MPWS experiments, the measurements were generally below the conservative estimate of the detection limit. However, in the "high C_0" experiment, there was a statistically significant peak beginning between 1 and 2 DPV (Figure 5.12), and the recovery was consistent with those from the other MPWS experiments, which were approximately an order of magnitude smaller than for the PWS. The recoveries were also consistent with those for thorium. However, unlike thorium, the plutonium(IV) high mobility form could not be definitively characterized as being particulate. In the batch filtration experiments (Figure 5.13 and Appendix F), approximately 60% was larger than 20 nm; and in the "high C_0" experiments, approximately 20–30% of the plutonium(IV) in the column effluent was larger than 12 nm. Speciation modeling of the spiked PWS (Meyers, 1999) within an E_H-pH envelop typical of natural waters predicted $Pu(OH)_4$ to be the predominant solid phase. Modeling results are presented in Appendix G.

Neptunium and Plutonium(V)

Breakthrough curves for neptunium under the influence of the PWS (solid symbols in Figure 5.14) were similar to americium, thorium and plutonium(IV) in that they were characterized by a small component (<<1%) with high mobility and a large component (≈50%) with intermediate mobility. However, there were differences as well. One difference is that the tailing edge of neptunium's intermediate mobility component did not decrease monotonically but instead had a small peak around 100 DPV. Also, neptunium's high mobility component took the form of a well-defined peak, and the recovery was considerably larger than those for americium, thorium, or plutonium(IV). Even greater differences were observed for the MPWS. Whereas the intermediate mobility component for americium, thorium, and plutonium(IV) almost disappeared, it

Table 5.5. Recoveries and Retardation Factors for the Plutonium(IV) Intermediate Mobility Component

Simulant	Recovery (3 – 1000 DPV)	Retardation Factor
PWS 1	0.610	79
PWS 2	0.620	35
MPWS 1	0.012	N/A
MPWS 2	0.006	N/A

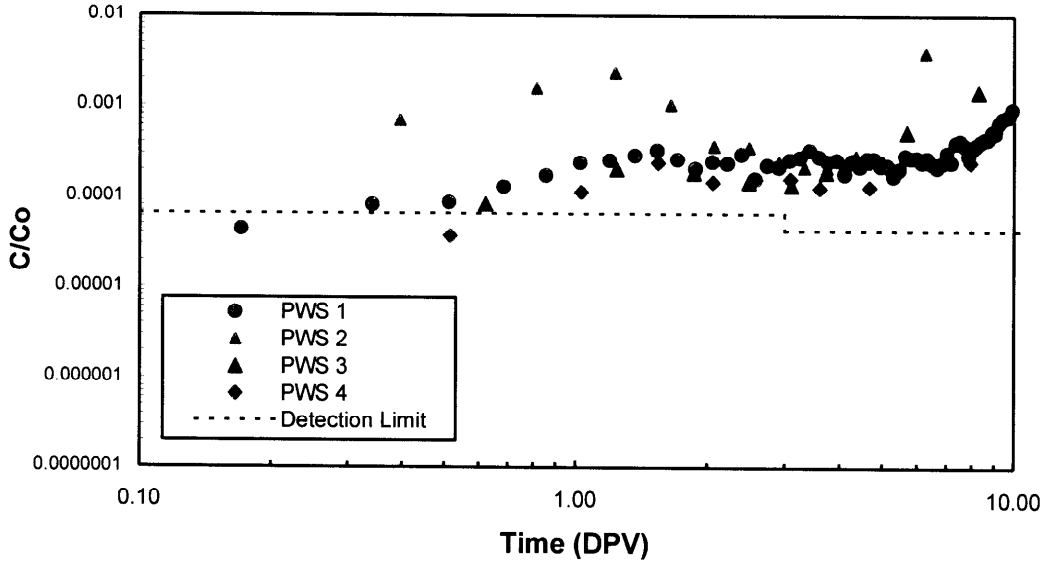

Figure 5.10. Expanded view of high mobility time period for plutonium(IV) for the PWS

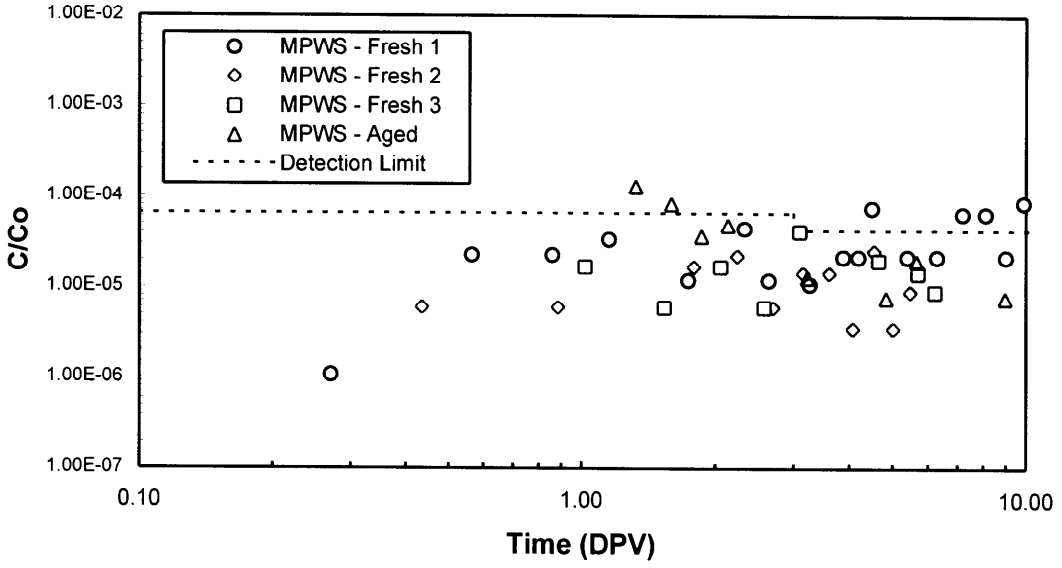

Figure 5.11. Expanded view of high mobility time period for plutonium(IV) for the MPWS

Table 5.6. Recoveries for the Plutonium(IV) High Mobility Component

Simulant	Recovery (< 5 DPV)
PWS 1	0.000700
PWS 2	0.002300
PWS 3	0.000340
PWS 4	0.000038
MPWS – Fresh 1	0.000030
MPWS – Fresh 2	0.000030
MPWS – Fresh 3	0.000017
MPWS – Aged	0.000050
MPWS – High C_0	0.000028

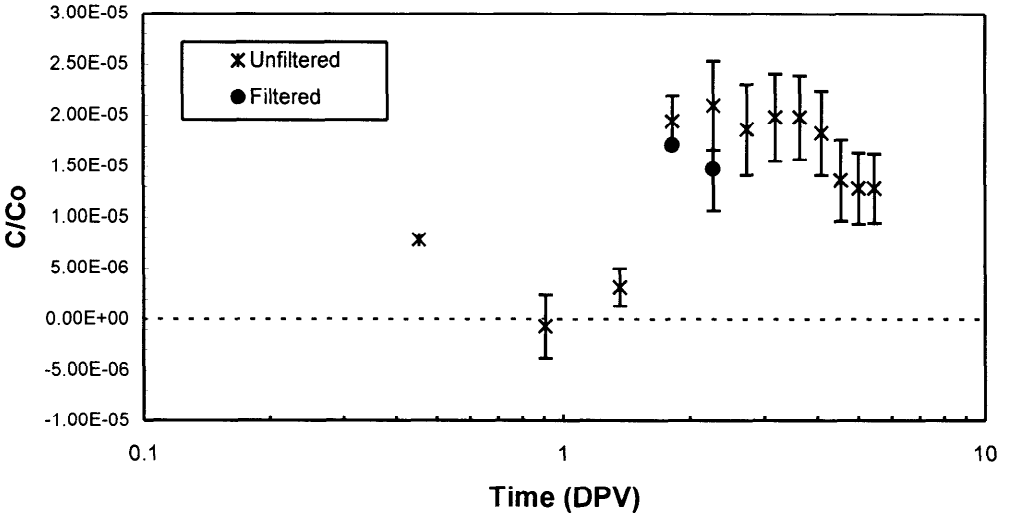

Figure 5.12. Plutonium(IV) high mobility component for an elevated C_0 – unfiltered and filtered (> 12 nm) analyses

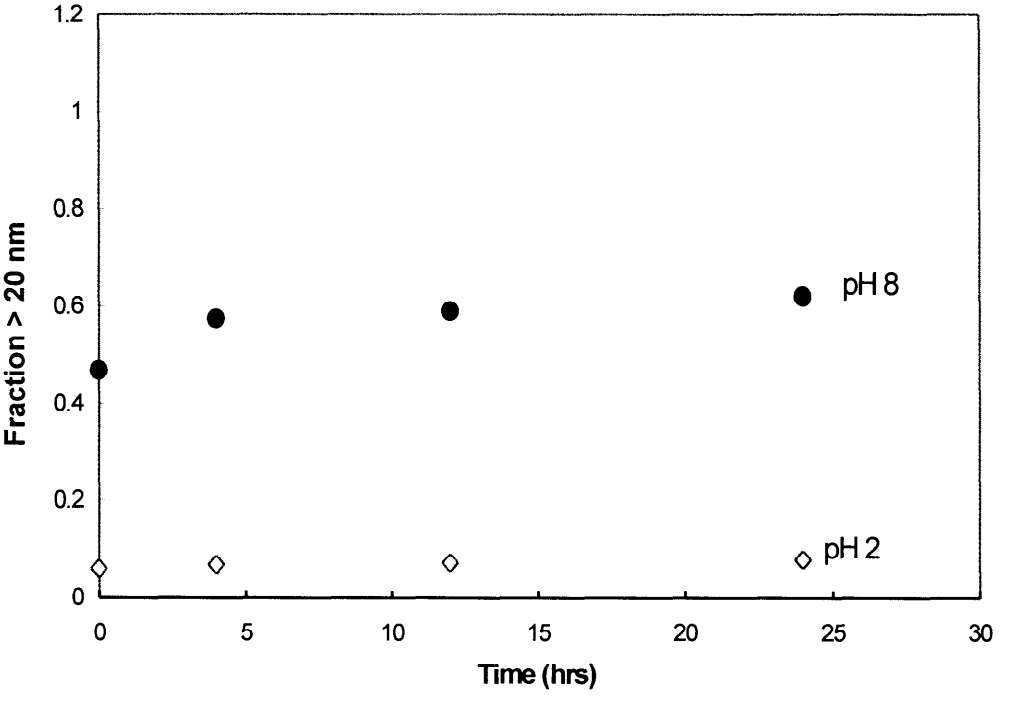

Figure 5.13. Particulate fraction as a function of aging time for plutonium(IV)

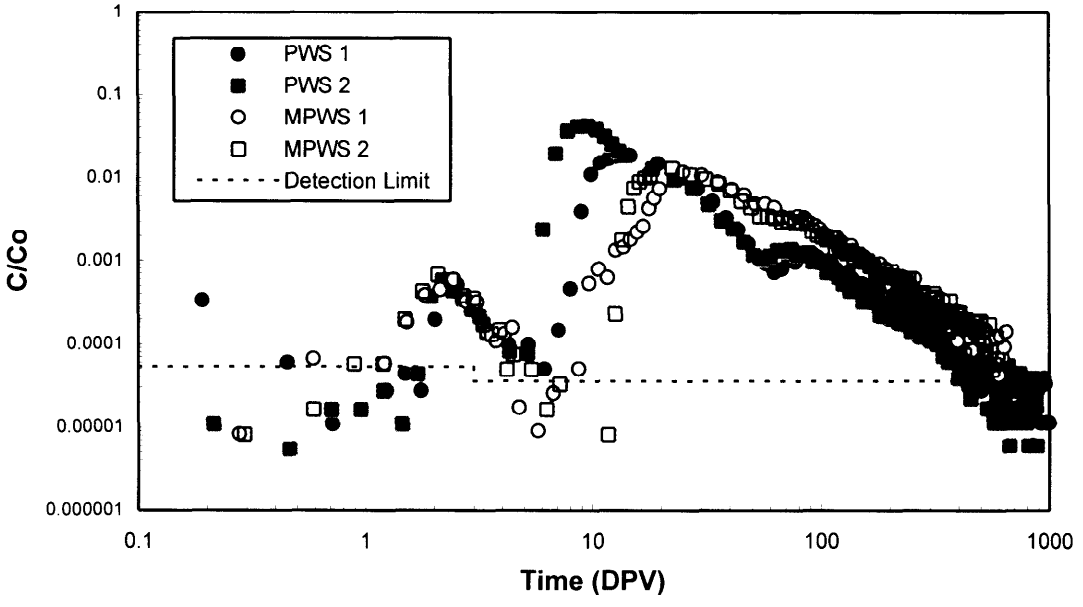

Figure 5.14. Neptunium breakthrough curves

showed little change for neptunium. Because of this, tests were conducted in which the ligands most likely to form complexes with neptunium were systematically removed from the PWS. Presented in Figure 5.15 are breakthrough curves for the PWS with CO_3^{2-}, F^-, and SO_4^{2-} removed independently. Qualitatively, there was very little change with the removal of F^- or SO_4^{2-} other than slight lateral shifts of the curves. However, removal of CO_3^{2-} resulted in striking changes. The high mobility component totally disappeared, and there was a significant change in the shape of the intermediate mobility component. Rather than peaking in the 10–30 DPV range, the intermediate mobility peaked near 100 DPV. In addition, the tailing edge decreased monotonically. These results suggested that CO_3^{2-} may play a role both in the high mobility component and in the 10–30 DPV peak in the intermediate mobility component.

To determine if either F^- or SO_4^{2-} plays a role in the 100 DPV peak, column experiments were conducted in which CO_3^{2-} was removed from the MPWS in combination with F^- and in combination with SO_4^{2-}. The breakthrough curves for these experiments are presented in Figure 5.16. The 100 DPV peak was still prominent, indicating that it is influenced by neither F^- nor SO_4^{2-}. Although these experiments were negative with respect to the 100 DPV peak, they may have revealed some more subtle influences. For the test with F^- and CO_3^{2-} removed, there was a peak during the 10–30 DPV time period (somewhat smaller than those in Figures 5.14 and 5.15). Yet, there was no peak when SO_4^{2-} was present along with F^- (and CO_3^{2-} removed) in Figure 5.15. This could occur if F^- is a stronger complexing agent than SO_4^{2-} with neptunium. The lack of sufficient thermodynamic data preclude modeling of the system. However, in the background section it is noted that the relative complexing strengths of common ligands with the actinides are ordered as $OH^- > F^- > SO_4^{2-}$. This suggests the possibility that the 100 DPV peak might be due to a neptunium hydroxide complex.

The expanded breakthrough curves are presented in Figure 5.17 and the "high C_0" curve is presented in Figure 5.18. In Figure 5.17, the circles and polygons represent experiments with CO_3^{2-} present and the various crossed symbols represent experiments with CO_3^{2-} removed. These data firmly establish a link between the high mobility component and CO_3^{2-}. The high mobility recovery was reproducible, ranging between

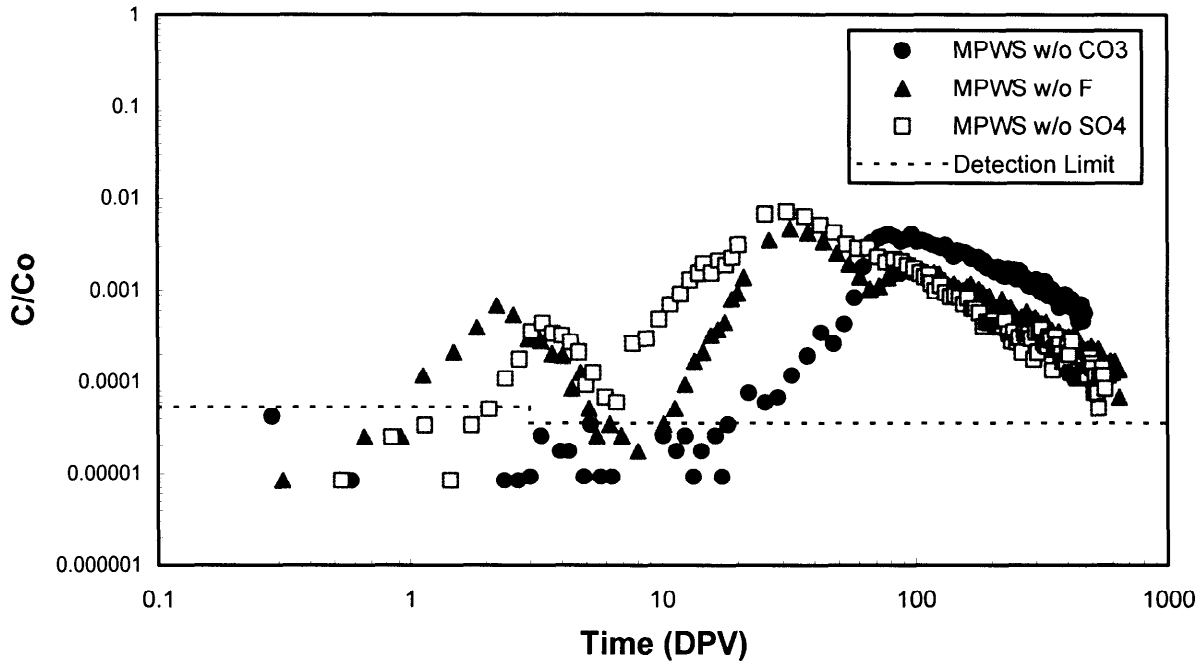

Figure 5.15. Effect of removing CO_3^{2-}, F^-, and SO_4^{2-} on neptunium breakthrough curves

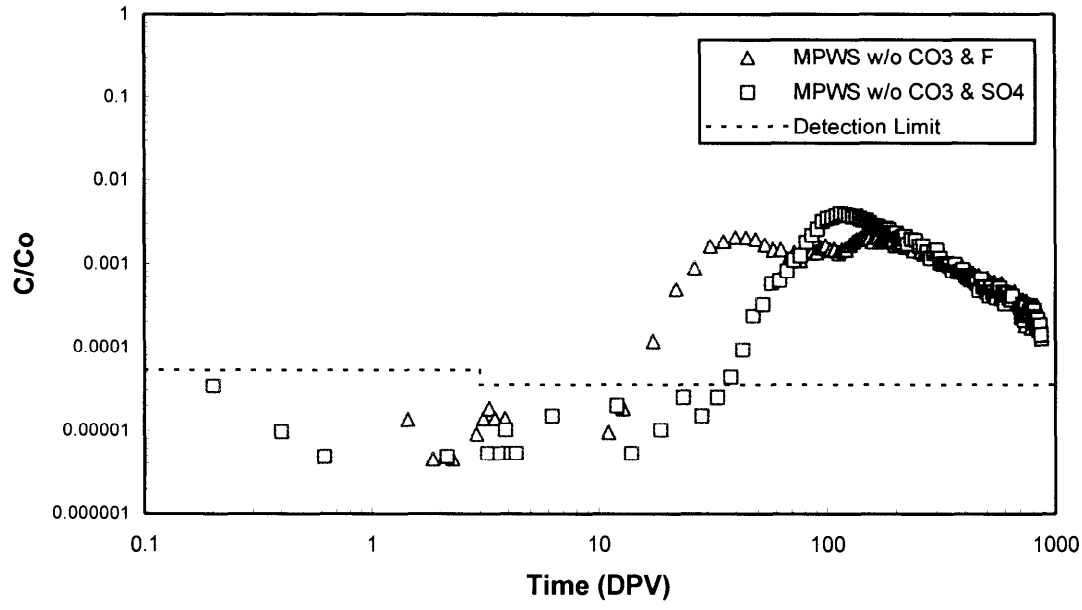

Figure 5.16. Effect of removing CO_3^{2-}, CO_3^{2-} & F^-, and CO_3^{2-} & SO_4^{2-} on neptunium breakthrough curves

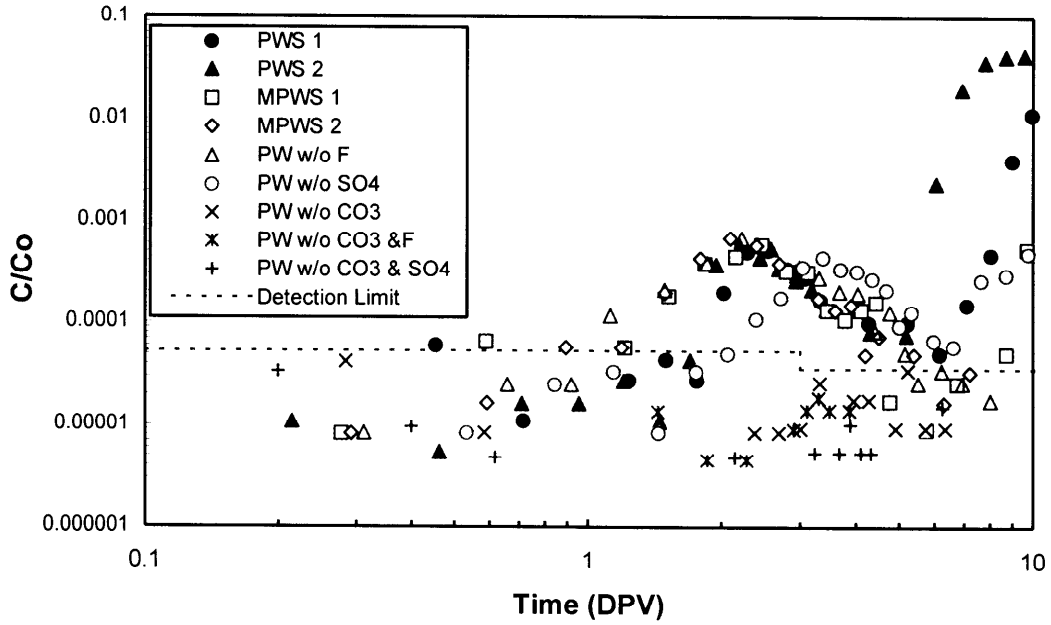

Figure 5.17. Expanded view of high mobility time period for neptunium

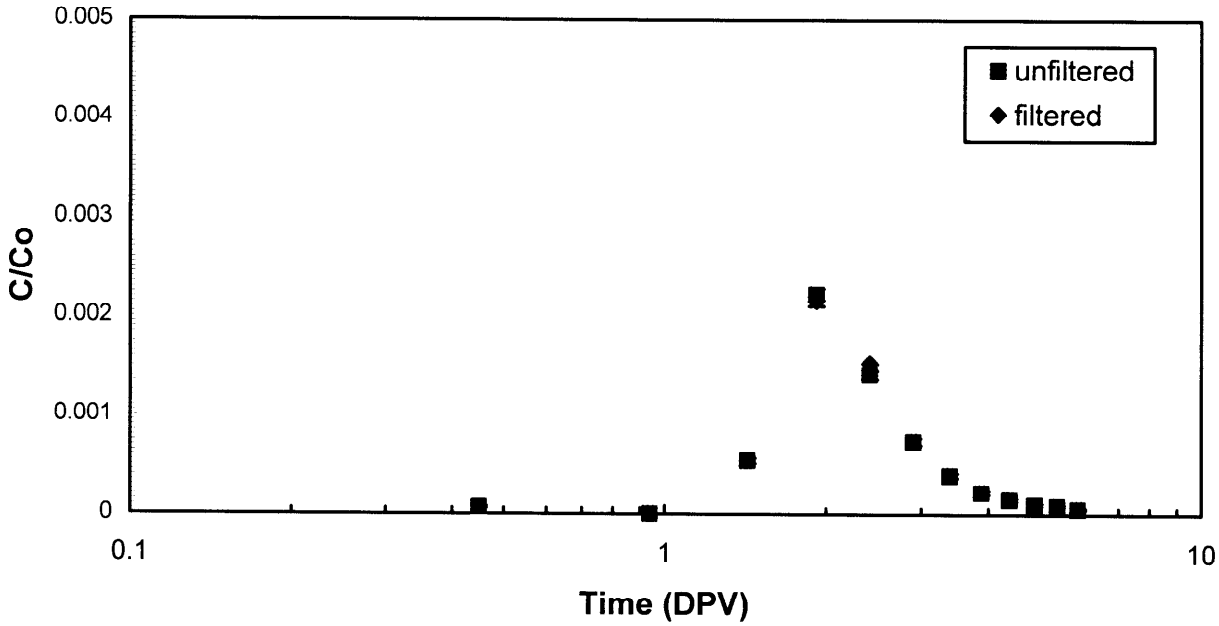

Figure 5.18. Neptunium high mobility component for an elevated C_0 – unfiltered and filtered (> 12 nm) analyses

0.00078 and 0.0010, and it was not affected by the removal of HA/EDTA, F^-, or SO_4^{2-} (Table 5.7). Retardation factors for the high mobility component varied from 1.3 to 3.8. The "high C_0" data for neptunium (Figure 5.18), similar to americium, illustrate the significance of the high mobility component. Also similar to americium, the filtered and unfiltered concentrations were the same, indicating that the high mobility component is either soluble or very small particles (<12 nm).

Although the retardation factors for the intermediate mobility component were quite variable (Table 5.7), they are consistent with the qualitative observations above; *i.e.* they increased when CO_3^{2-} was removed. The recoveries for the intermediate mobility component were also quite variable, due both to variability in the eluent chemistries and to truncation of some experiments before the effluent concentrations returned to background levels. The latter is clearly evident in Figure 5.16, where the effluent concentrations were more than an order of magnitude above background (5×10^{-6}) when the experiments were terminated. In experiments which were not terminated until background was reached the maximum recovery was 80%, and the typical recovery was around 60%. This implies recoveries for the low mobility component to be between 20 and 40%. One hypothesis for the low mobility component is reduction of some of the neptunium(V) to neptunium(IV) by reduced iron or manganese in the interbed material. Neptunium(IV) is highly insoluble and would have very low mobility (Brookins, 1988). To test this hypothesis, experiments were conducted under oxidizing conditions as described in the Materials and Methods section. The breakthrough curves for these tests are presented in Figure 5.19. These curves are similar to those in Figure 5.15 with the exception that, within the limits of experimental uncertainty, all of the neptunium in the spike was recovered (Table 5.8). This is supportive of the neptunium(V) to neptunium(IV) reduction hypothesis.

Presented in Figure 5.20 are column effluent data for plutonium(V) for the PWS and for the MPWS. Also included are background data obtained for an unspiked column. The ordinate is the gross count rate rather than the normalized concentration to facilitate comparisons with background. In contrast to neptunium(V), there was very little breakthrough of plutonium(V) - over 99.99% of the plutonium(V) was retained in the columns. This notwithstanding, there were sporadic releases of very small amounts of plutonium from the columns throughout the duration of the experiments. Since these releases were not characterized, we refrain from speculating about their physical/chemical form. However, this behavior is consistent with the sporadic

Table 5.7. Retardation Factors and Recoveries for Neptunium

Simulant	High Mobility			Intermediate Mobility	
	Range	R	Recovery	R	Recovery
PWS 1	< 7 DPV	2.5	0.00100	80	0.57
PWS 2	< 5 DPV	2.2	0.00078	58	0.67
MPWS 1	< 5 DPV	2.1	0.00093	104	0.68
MPWS 2	< 7 DPV	1.3	0.00100	99	0.64
MPWS w/o F^-	< 6 DPV	2.7	0.00100	156	0.40
MPWS w/o SO_4^{2-}	< 7 DPV	3.8	0.00078	97	0.41
MPWS w/o CO_3^{2-}	N/A	N/A	0.0	195	0.69
MPWS w/o CO_3^{2-} & F^-	N/A	N/A	0.0	237	0.67
MPWS w/o CO_3^{2-} & SO_4^{2-}	N/A	N/A	0.0	310	0.81

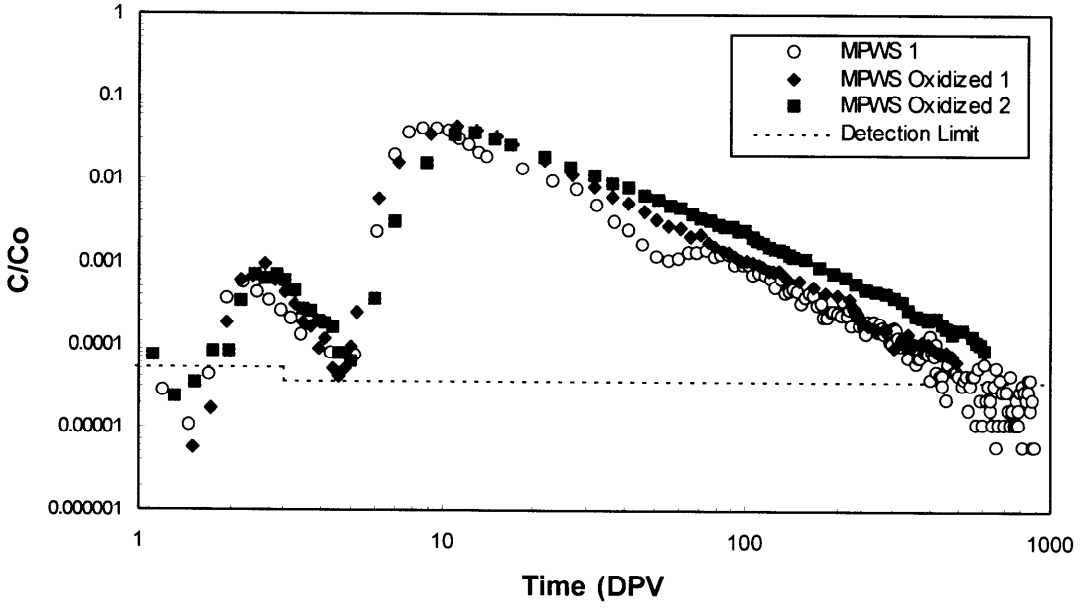

Figure 5.19. Neptunium breakthrough curves under oxidizing conditions

Table 5.8 Retardation Factors and Recoveries for Neptunium Under Oxidizing Conditions

	High Mobility Component		Intermediate Mobility Component	
Experiment	R	F	R	F
Oxidizing #1	1.6	0.0010	265	0.90
Oxidizing #2	1.5	0.0013	434	1.07

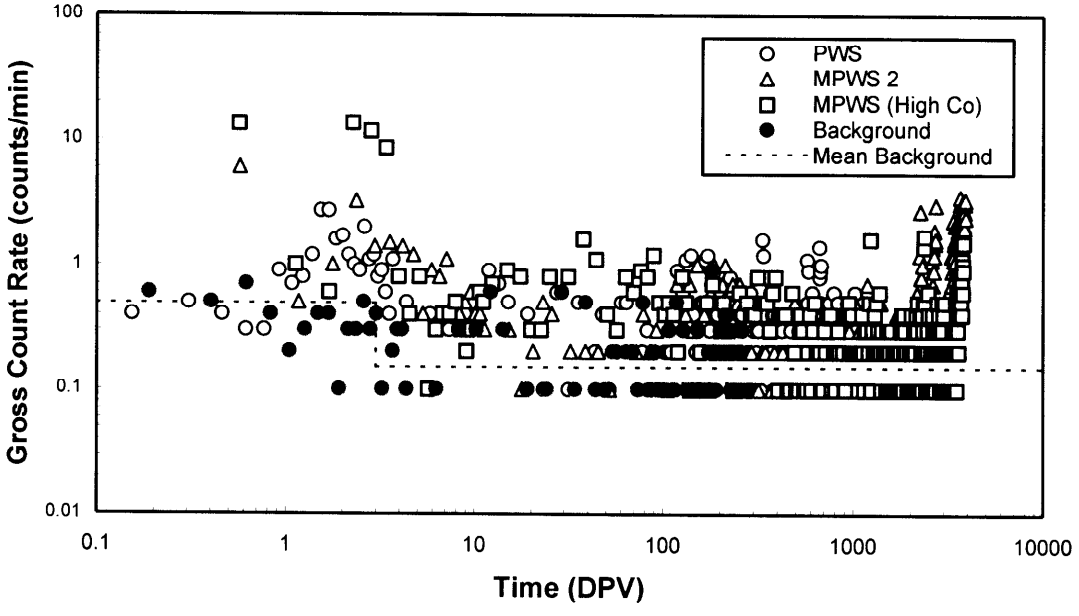

Figure 5.20. Plutonium(V) breakthrough curves

occurrence of americium and plutonium in monitoring data and with the stochastic nature of colloidal transport. There was a high mobility component, but it was smaller and less prominent than for neptunium. In two of these tests, changes in eluent chemistry were made between 2000 DPV and 3000 DPV. The first change was from pH8 to pH2 around 2300 DPV and the second was from pH2 to pH1 around 2700 DPV. These changes resulted in small increases in breakthrough, likely due to solubilization of plutonium hydroxide before the polymeric oxy-hydroxide formed.

The expanded breakthrough curves are presented in Figure 5.21. For the < 1 DPV time period, no breakthrough was apparent in two of the experiments and there was the possibility of breakthrough in the other two. For the 1–10 DPV period, there was a small amount of breakthrough in all of the experiments. Recoveries for discrete time periods are given in Table 5.9. For the 1–10 and 10–100 DPV time periods, the fractions were rather consistent, varying between 10^{-4} and 10^{-3}. The variability was larger, 10^{-5} to 10^{-3}, for the < 1 DPV period. They were not consistent for the other two time periods. The "high C_0" data are presented in Figure 5.22. Although there is definitely some breakthrough, it is very small. The filtered samples from the 1–2 DPV time period differed significantly from the unfiltered samples, indicating a mixture of species larger and smaller than 12 nm.

Based on the evidence presented above for reduction and subsequent immobilization of neptunium(V), the same mechanism was hypothesized for plutonium(V). Since plutonium(V) is more readily reduced than neptunium, it is possible that almost all of the plutonium is reduced rather than part of it as for neptunium. Presented in Figure 5.23 are breakthrough curves for experiments conducted under oxidizing conditions. Breakthrough did not increase under oxidizing conditions as it did for neptunium. This was not surprising given that plutonium(V) is more easily reduced than neptunium(V), and the reduction potential of the column effluent was below that required for plutonium(V) to be the predominant species.

Uranium

Breakthrough curves for uranium under the influence of the MPWS (experiments were not conducted for uranium with the PWS) are presented in Figure 5.24. These curves, in contrast to those for the other actinides, were characterized by a single peak containing all of the activity in the spike. Breakthrough began immediately, peaked

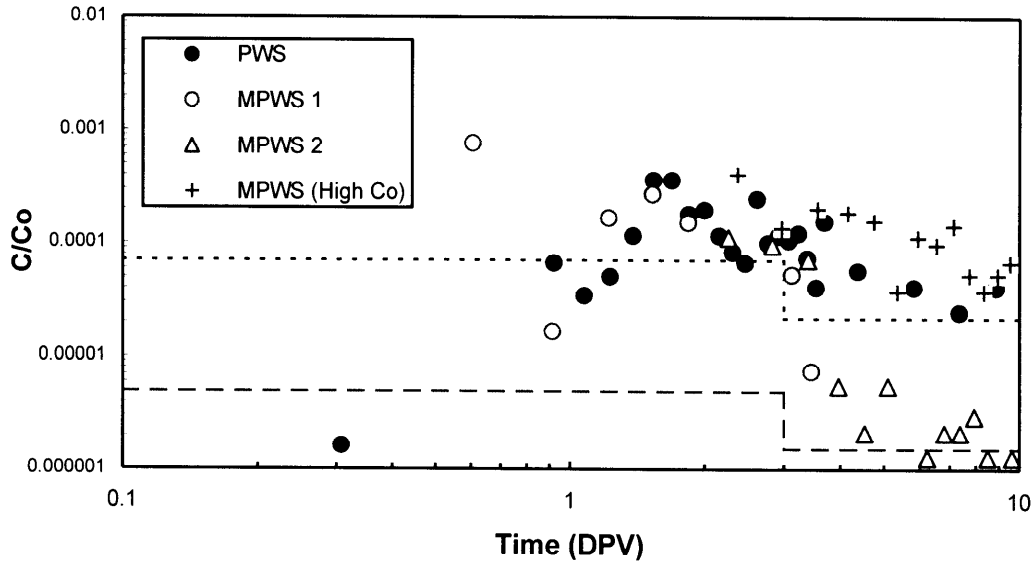

Figure 5.21. Expanded view of high mobility time period for plutonium(V)

Table 5.9. Plutonium(V) Recoveries for Discrete Time Periods

Experiment	Time Period (DPV)				
	< 1	1 – 10	10 – 100	100 – 1000	> 1000
PWS	2.7×10^{-5}	8.5×10^{-4}	6.9×10^{-4}	1.5×10^{-2}	N/A
MPWS 1	9.7×10^{-4}	1.8×10^{-4}	N/A	N/A	N/A
MPWS 2	3.6×10^{-4}	7.1×10^{-4}	5.1×10^{-4}	-2.5×10^{-5}	1.2×10^{-1}
MPWS (high C_0)	4.8×10^{-5}	1.3×10^{-4}	3.2×10^{-4}	3.1×10^{-4}	3.1×10^{-4}

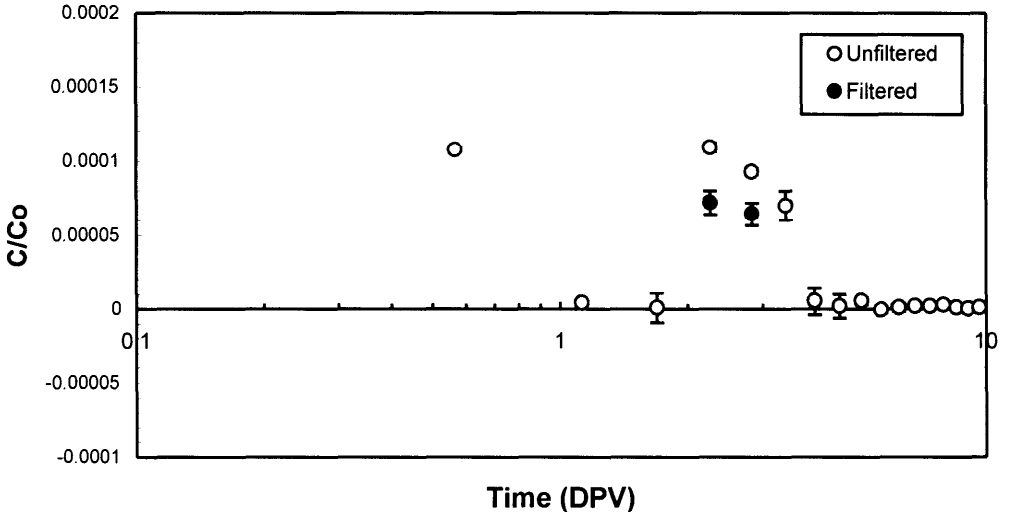

Figure 5.22. Plutonium(V) high mobility component for an elevated C_0 – unfiltered and filtered (>12 nm) analyses

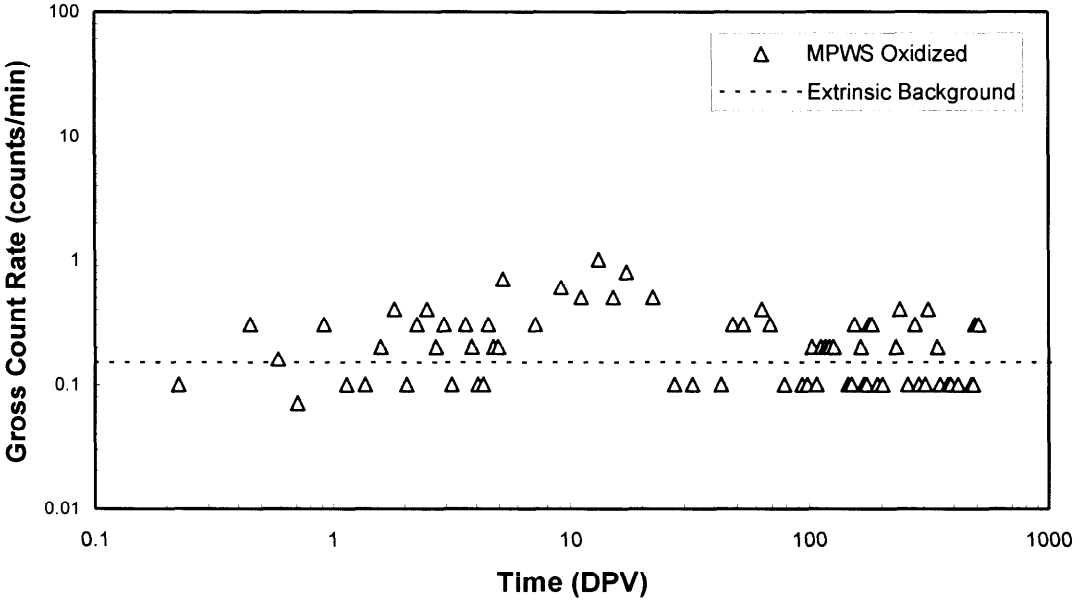

Figure 5.23. Plutonium(V) breakthrough curves under oxidizing conditions

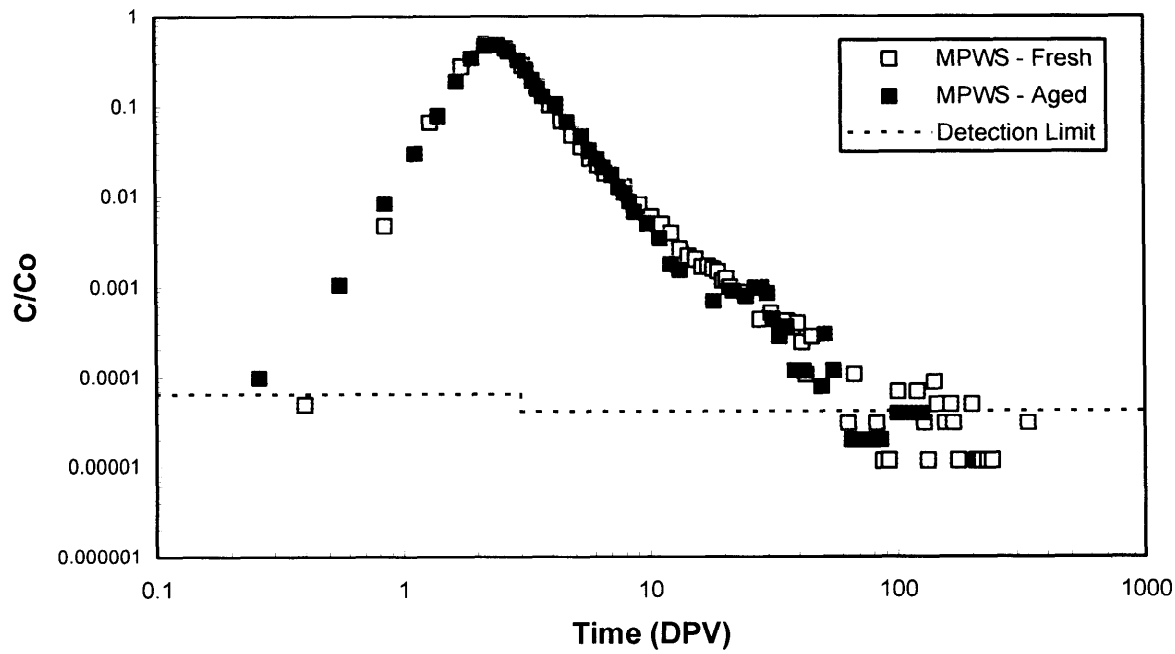

Figure 5.24. Uranium breakthrough curves

between 2 and 3 DPV, and was complete within 100 DPV. This behavior was not significantly affected by the removal of either F- or SO_4^{2-} (Figure 5.25). However, it was greatly affected by the removal of CO_3^{2-}, which resulted in two distinct peaks, a small one at 10 DPV and a large one at 200 DPV. The peak at 10 DPV disappeared when CO_3^{2-} was removed in combination with F^- and when it was removed in combination with SO_4^{2-} (Figure 5.26). The leading edge of the peak at 200 DPV became sharper with the removal of F^- and sharper still with the removal of SO_4^{2-}, but the tailing edge did not change appreciably. Retardation factors and recoveries for the uranium experiments are presented in Table 5.10. For MPWS – fresh, MPWS – aged, MPWS w/o F^-, and MPWS w/o SO_4^{2-}, the experiments were not terminated until the concentrations reached background and the recoveries exceeded 90%. The other experiments were truncated before background was reached, and the recoveries varied from 73 to 77%. Although the missing uranium was probably contained in the truncated portion of the curve, the experiments would have to extended to almost 10,000 DPV to verify this.

The breakthrough curves clearly indicate that a carbonate species is responsible for uranium transport under the influence of the MPWS. This is consistent with modeling results (Table 5.11), which predict $UO_2(CO_3)_3^{4-}$ and $UO_2(CO_3)_2^{2-}$ as the predominant species for the MPWS. When CO_3^{2-} is removed from the MPWS, the model predicts $UO_2(OH)_2$ and $UO_2(OH)_3^{1-}$ to dominate. Thus, the 200 DPV peak is likely due to the hydroxide species. Removal of F^- and SO_4^{2-}, in both the presence and absence of CO_3^{2-}, did not appreciably affect the speciation.

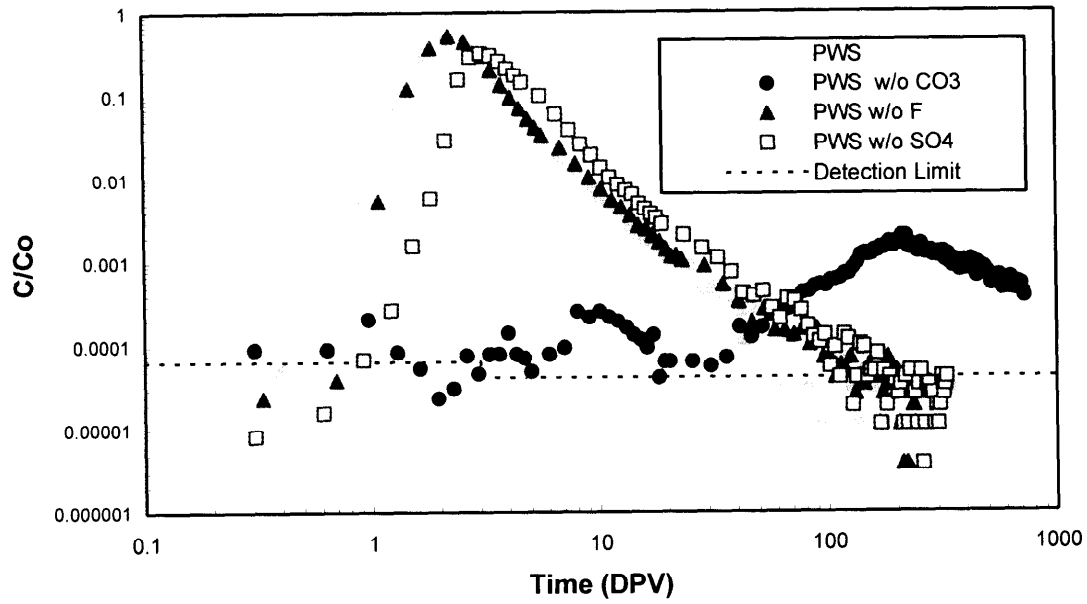

Figure 5.25. Effect of removing CO_3^{2-}, F^-, and SO_4^{2-} on uranium breakthrough curves

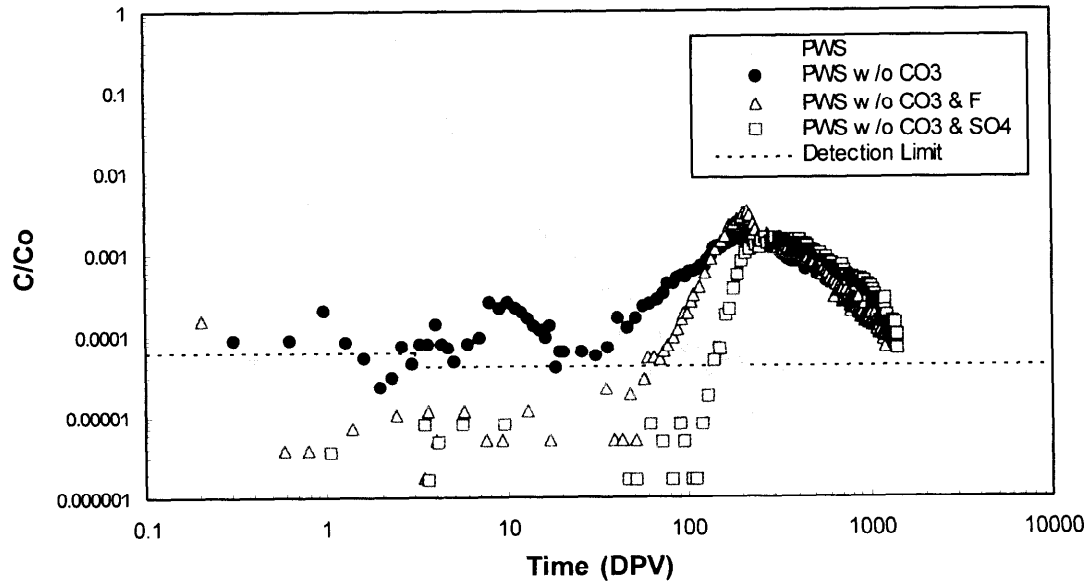

Figure 5.26. Effect of removing CO_3^{2-}, CO_3^{2-} & F^-, and CO_3^{2-} & SO_4^{2-} on uranium breakthrough curves

Table 5.10. Uranium Recoveries and Retardation Factors

Simulant	Time Period (DPV)	Recovery	R
MPWS – Fresh	0 – 100	0.91	3.2
MPWS – Aged	0 – 100	0.96	3.9
MPWS w/o F^-	0 – 240	0.93	5.1
MPWS w/o SO_4^{2-}	0 – 330	0.95	8.2
MPWS w/o CO_3^{2-}	5 – 20	0.002	12
	20 – 800	0.45	340
MPWS w/o CO_3^{2-} and F^-	20 – 1220	0.77	690
MPWS w/o CO_3^{2-} and SO_4^{2-}	20 – 1445	0.73	560

Table 5.11. Speciation Modeling Results for Uranium

	% Distribution			
RUN	$UO_2(CO_3)_2^{-2}$	$UO_2(CO_3)_3^{-4}$	$UO_2(OH)_2$	$UO_2(OH)_3^{-1}$
allow pptn	7.3	92.7	neg	neg
pptn excluded	7.0	93.0	neg	neg
(all below pptn excluded, but no change if allowed)				
+1.3 mg/l EDTA	7.0	93.0	neg	neg
(note: U-EDTA species < ~10^{-30} M; EDTA tied up with Ca and Mg)				
no F^-	7.2	92.8	neg	neg
no CO_3^{2-}	neg	neg.	87.0	12.8
no SO_4^{2-}	7.6	92.4	neg	neg
no SO_4^{2-}, CO_3^{2-}	neg	neg	87.1	12.7